ELSEVIER

Journal of Neuroscience Methods 152 (2006) 32–39

JOURNAL OF NEUROSCIENCE METHODS

www.elsevier.com/locate/jneumeth

# Automated criteria-based selection and analysis of fluorescent synaptic puncta

Jeremy B. Bergsman *, Stefan R. Krueger, Reiko Maki Fitzsimonds

*Department of Cellular and Molecular Physiology, Yale University School of Medicine, 333 Cedar St. SHM B 144, New Haven, CT 06510, USA*

Received 27 April 2005; received in revised form 10 August 2005; accepted 11 August 2005

**Abstract**

The use of fluorescent probes such as FM 1-43 or synapto-pHluorin to study the dynamic aspects of synaptic function has dramatically increased in recent years. The analysis of such experiments is both labor intensive and subject to potentially significant experimenter bias. For our analysis of fluorescently labeled synapses in cultured hippocampal neurons, we have developed an automated approach to punctum identification and classification. This automatic selection and processing of fluorescently labeled synaptic puncta not only reduces the chance of subjective bias and improves the quality and reproducibility of the analyses, but also greatly increases the number of release sites that can be rapidly analyzed from a given experiment, increasing the signal-to-noise ratio of the data. An important innovation to the automation of analysis is our method for objectively selecting puncta for analysis, particularly important for studying and comparing dynamic functional properties of a large population of individual synapses. The fluorescence change for each individual punctum is automatically scored according to several criteria, allowing objective assessment of the quality of each site. An entirely automated and thus unbiased analysis of fluorescence in the study of synaptic function is critical to providing a comprehensive understanding of the cellular and molecular underpinnings of neurotransmission and plasticity.


*Keywords:* Fluorescence; Synaptic; Automation; FM 1-43; Plasticity; Neurotransmission

## 1. Introduction

Synapses exhibit a remarkable degree of functional diversity generated by genetically predetermined mechanisms as well as activity-dependent modifications. The use of digital microscopy to visualize fluorescent reporters of cellular structures in living neurons has revolutionized our understanding of the processes leading to functional synaptic diversity by enabling us to study the function of individual synapses. In particular, monitoring of synaptic vesicle cycling with styryl dyes such as FM 1-43 (Betz and Bewick, 1992), and genetically encoded fluorescently tagged proteins such as synapto-pHluorin (Miesenböck et al., 1998) has allowed for the measurement of the function of individual presynaptic terminals. These techniques have been extensively used to study many fundamental aspects of synapse formation and modulation (see review, Miesenböck, 2004).

We routinely examine the localization and recycling of synaptic vesicles at presynaptic release sites in low-density cultures of hippocampal neurons using FM 1-43 as a fluorescent reporter. Analyses of the initial fluorescence intensity of FM 1-43 loading as well as the kinetics of destaining in response to electrical field stimulation are critical measurements used to understand the presynaptic properties of neurotransmission and plasticity. The analysis of such experiments is labor-intensive, especially if data from large numbers of presynaptic release sites need to be obtained to yield statistically meaningful datasets. The multistep processing of time-lapse wide field microscopy images of synaptic vesicle cycling includes subtraction of background fluorescence (e.g. Miesenböck, 2000) and registration of images to correct for movement during an experiment. Typically, labeled release sites are then selected manually by exploration of a baseline image for fluorescent puncta of appropriate sizes followed by a subjective drawing or placement of a region of interest (ROI) over the punctum. Finally the fluorescence values of the puncta are measured over the course of the experiment.

In addition to being labor-intensive, the analysis of FM1-43 destaining experiments is subject to potentially significant experimenter bias. The most critical step in analyzing fluorescent images of presynaptic function in this respect is the accurate identification and selection of discrete sites of vesicle cycling.

* Corresponding author. Tel.: +1 203 785 3157; fax: +1 203 785 4951.
*E-mail address:* jeremy@bergsman.org (J.B. Bergsman).

0165-0270/$ – see front matter © 2005 Elsevier B.V. All rights reserved.
doi:10.1016/j.jneumeth.2005.08.008

An experimenter-initiated selection process may introduce bias, as it critically (and perhaps unrealistically) depends upon consistent, rigorous, and accurate application by eye of explicit and implicit criteria such as initial fluorescence intensity, overall size of the fluorescent puncta, and physical characteristics of the neuritic processes to every punctum in the image. Selection bias can further be exacerbated by the fact that meaningful staining can occur across a wide range of intensities (Krueger et al., 2003), which can be difficult to resolve by eye without repetitive adjustment or thresholding of the image display. These types of issues are a general problem in image processing, and have been addressed previously in many different semi-automated and fully automated approaches (for review see Pal and Pal, 1993; Sahoo et al., 1988). However, no general solution for all types of images is known. A somewhat similar approach for analysis of fluorescent synaptic puncta written in interactive data language (IDL) has been previously developed (Zakharenko et al., 2002).

Here we describe an automated approach to analyzing such experiments, utilizing freely available routines that automatically process and analyze images of fluorescently labeled synaptic puncta. This substantially reduces the user time required for such analysis and, more importantly, improves the quality, quantity, and reproducibility of the analyzed data. In addition, we have developed an automated process to score the fluorescence changes for each punctum according to several criteria assessing the quality of the data. In this way, it is possible to exclude objectively data of low quality, such as release sites undergoing a high degree of spontaneous release or fluorescence signals with unfavorable signal-to-noise ratio, from further analysis.

Our routines comprise a set of functions that runs within the commercial scientific data analysis program Igor Pro. Image file formats from the commercial programs IPLab and Wasabi, as well as the general purpose TIFF format can be analyzed. Our functions produce well-organized output that can be easily manipulated to produce publication-quality figures, all within Igor Pro. Our Igor Pro routines are open source, allowing users to verify their operation and modify them for their own purposes. In the present analysis, we have applied this method to punctate fluorescent images of presynaptic release sites; however the routines are adaptable to the analysis of a wide range of fluorescent images. For our application, we demonstrate that the automatic criteria-based selection of release sites not only reduces the chance of subjective bias, but also greatly increases the number of release sites that can be analyzed from a given experiment, increasing the signal-to-noise ratio of the data.

## 2. Materials and methods

### 2.1. Cell culture

Mouse hippocampal neurons were cultured essentially as described in Krueger et al. (2003). Briefly, coverslips (Warner Instruments, Hamden, CT) were coated for 45 min with 0.05% (w/v) poly-L-lysine (Peptides International, Louisville, KY) and then overnight or longer with 4 μg/ml mouse laminin (Gibco/Invitrogen, Carlsbad, CA). Before use they were washed twice with water and once with Neurobasal A (Gibco) medium supplemented with B-27 (Gibco), 2 mM glutamine, 1 mM pyruvate, and 5% fetal calf serum (Hyclone, Logan, UT). Hippocampi were dissected from mouse pups (P0-P1), incubated for 30 min with 0.01% papain (Worthington, Lakewood, NJ), 0.1% dispase II (Roche, Indianapolis, IN), and 0.01% DNAse I, and dissociated using fire-polished Pasteur pipettes. Cells were then plated at a density of 3000 $cm^{-2}$ in the above medium, then, 2–3 h after plating, the cells were washed once with the same medium without serum. After 2–3 days 4 μM Ara-C was added to limit glial proliferation. The neurons were plated at a very low density to prevent fasciculation of the neurites, a problem that interferes with unambiguous optical separation of the fluorescently labeled release sites. Unless otherwise indicated, chemicals were from Sigma (St. Louis, MO).

### 2.2. Fluorescence microscopy and imaging

Fluorescence microscopy was performed using a Nikon TE300 inverted epifluorescence microscope equipped with a Nikon 40X, 0.75 NA objective, a Uniblitz shutter, and a fluorescence filter set (Chroma, Brattleboro, VT) for FM 1–43 (480/40 nm bandpass excitation, 505 nm longpass beamsplitter; 515 nm longpass emission). Images were acquired with a Hamamatsu (Bridgewater, NJ) ORCA CCD camera controlled by IPLab software (Scanalytics, Fairfax, VA). During experiments, cells were perfused at room temperature with HEPES-buffered saline (HBS) containing (in mM) 124 NaCl, 3 KCl, 2 $CaCl_2$, 1 $MgCl_2$, 10 HEPES, and 5 D-glucose, adjusted to pH 7.3, supplemented with 10 μM 6,7-dinitroquinoxaline-2,3-dione and 50 μM 2-amino-5-phosphonopentanoic acid to prevent recurrent excitation. Action potentials were elicited by passing 1 ms current pulses yielding fields of 10–12 V $cm^{-1}$ through platinum electrodes placed ~0.9 cm apart. Images were acquired at a rate of 1 Hz initially and then at 0.2 Hz later in the experiment to minimize photodamage when fluorescence changes were slower. All chemicals were from Sigma except as indicated.

### 2.3. Hardware and software requirements

The set of routines described in this paper is open source and available for use under the GNU General Public License (http://www.gnu.org/copyleft/gpl.html). The code and a detailed user's manual can be obtained as supplemental information to this paper; the most recent versions are available from the corresponding author's web site (http://bergsman.org/jeremy/Igor/default.html). The routines run within Igor Pro (Wavemetrics, http://www.wavemetrics.com), version 5.03 or higher. Igor Pro runs on both Macintosh and Windows operating systems. The software was developed on a 2.2 GHz Pentium 4 PC running Windows XP, and has been tested on other Windows machines and a 500 MHz PowerPC G4 Macintosh computer running OSX version 10.3.8. The software can read image files created by third party software from Scanalytics (IPLab, http://www.scanalytics.com) and Hamamatsu (Wasabi,

http://usa.hamamatsu.com/assets/pdf/hpspdf/Wasabi.pdf), as well as the standard image format TIFF. Finally, image data can be acquired directly with Igor Pro using additional software from Wavemetrics or third parties (http://www.wavemetrics.com/products/igorpro/imageprocessing/imageacquisition.htm). Image size, resolution, acquisition rate, and dynamic range are not limited by the program and are handled automatically.

## 3. Results

### 3.1. FM1-43 labeling of presynaptic release sites in cultured mouse hippocampal neurons

Recycling synaptic vesicles in cultured neurons were stained by 900 stimuli delivered at 10 Hz in the presence of 15 μM FM 1–43. After several minutes of perfusion with FM dye-free extracellular solution to wash away non-internalized dye, we imaged neurons while delivering another 900 stimuli at 10 Hz to cause activity-dependent release of previously internalized dye. Fifteen images were acquired at 1 Hz, with stimulation beginning after 10 baseline images. After a few seconds of stimulation the rate of fluorescence change generally decreases and the image acquisition rate was lowered to 0.2 Hz for the remaining 18 images to minimize photodamage. The experiment presented here as an example was unusual in not being ideal due to the presence of fine debris in the background, and was specifically chosen to illustrate the robustness of the approach to this potential source of artifact.

### 3.2. Image processing and automated selection of FM 1–43 labeled release sites

Upon starting the program within Igor Pro, a control panel is presented which allows the user to adjust the processing and analysis parameters (Fig. 1). The processing and analysis steps described below are applied to all the images in any number of experiments residing in a disk folder.

#### 3.2.1. Background subtraction

Light scatter and autofluorescence of medium and substrate create background fluorescence in wide-field microscopic images that is often inhomogeneous due to uneven illumination of the specimen. This background fluorescence has to be subtracted to allow for successful automated segmentation and to correct the measured intensities for spurious signal not derived from the fluorescent probe. For this purpose, our routines use an algorithm that divides each image in an experiment into squares of user-specified size. The dimmest pixel in each square is considered the background and a smooth 2D polynomial is fit to these points, which is then subtracted from that image. The results of this algorithm are superior to other frequently used background subtraction methods, such as the rolling ball algorithm (Sternberg, 1983) and the subtraction of a heavily smoothed image from the original (Miesenböck, 2000) in being less influenced by non-background objects and less likely to develop discontinuities.

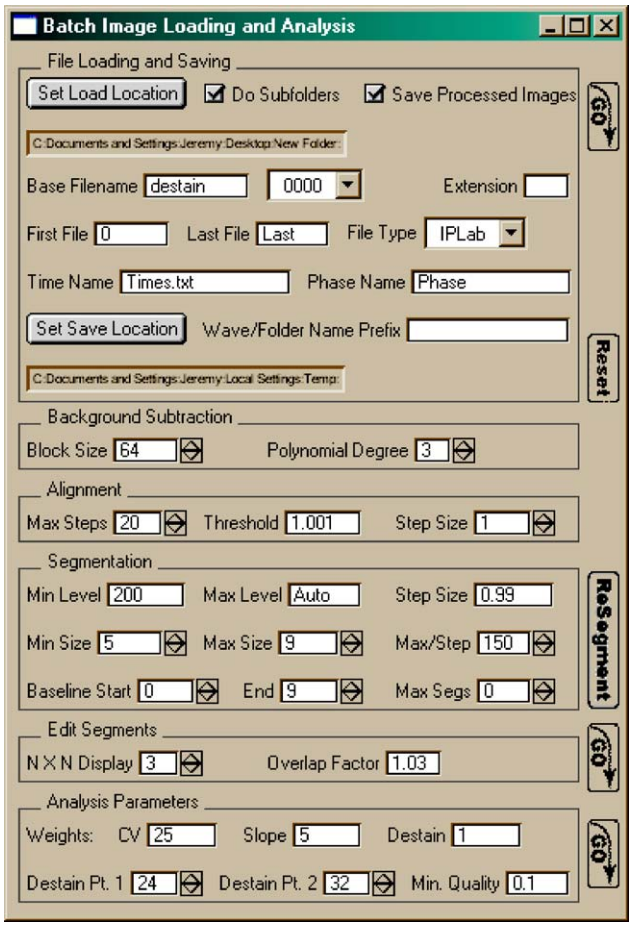


Fig. 1. Control panel for image processing allows the user to set the parameters that affect the processing.

#### 3.2.2. Alignment

Minor movements of specimen or microscope stage often lead to small shifts of the imaged field during time-lapse microscopy, necessitating alignment of individual images in a stack relative to the baseline image prior to analysis. For this purpose, the brighter areas in the averaged baseline image (the baseline is set in the segmentation parameters section described below) are identified and used as an ROI for the subsequent steps. Each image is translated in a series of stepwise movements in the *X* and *Y* directions to maximize its brightness in this ROI. There is no rotation or subpixel movement. Each step can be allowed to be one or more pixels in size, according to a user-supplied parameter. A shifted image must be brighter than the starting image by a user-specified amount to be accepted. The maximum number of steps allowed is also specified by a user-supplied parameter. By setting this parameter to zero, alignment changes are prevented, which allows the study of moving fluorescent areas. Allowing larger steps slows processing, but may be required for experiments with large specimen movement.

#### 3.2.3. Segmentation

Segmentation is the division of an image into regions of background and regions of interest. The ROI are the areas that will subsequently be analyzed for fluorescence changes. Auto-

mated segmentation is performed on a baseline set of images, which are averaged together to provide a lower noise image for segmentation by one of the methods described below. Typically, automated segmentation routines employ thresholding approaches (Sahoo et al., 1988), possibly followed by application of secondary techniques such as shape criteria, edge detection, or image morphology operations to isolate edges of objects with inhomogeneous intensity. Our routines provide as an option a simple implementation of this approach, as described in Supplementary Figure 1 (for a more advanced implementation, see Wahlby et al., 2004). While this method works well, for example, to identify individual cells filled with calcium indicators, it is insufficient for identifying release sites labeled with FM dyes or synapto-pHluorin. Stained release sites display a large range of fluorescence intensities, which differ little from nearby pixels due to partially stained and/or autofluorescent neuritic processes; they are also small and often clustered. All of these characteristics are troublesome for most threshold-based segmentation techniques. We therefore adopted an iterated thresholding approach that aims to find local maxima of fluorescence intensity that fit a size criterion. The image is repeatedly thresholded in discrete steps, from high to low intensity spanning most of the dynamic range of the image, selecting for contiguous areas over the current intensity threshold that meet the size parameters. Selected regions are accumulated for all intensity steps, and then re-screened for conformance with the size parameters. Successful segmentation depends on the choice of appropriate values for various parameters for the images being analyzed. Fig. 2A and B show examples of the application of two different size parameters to part of an image, and Fig. 2C and D show ROI (in red and white, see below) determined by our typical settings on a larger field. The settings of the various parameters as well as other relevant data for the analysis of the image shown in Fig. 2 are given in Table 1. A maximum intensity parameter allows areas that are too bright (e.g., due to saturation) to be avoided. Spurious identification of ROI in the background is avoided by two user-supplied parameter-driven strategies: (1) a minimum intensity parameter prevents analysis of regions of very low intensity, which tend not to be functional release sites and (2) a parameter which halts the segmentation when too many ROI are found in a given intensity band, a typical result when pixels within the background are being analyzed. The program allows easy resegmentation during an analysis, which facilitates the determination of an appropriate set of parameter values for general future use.

Table 1

| Parameter | Value |
|---|---|
| Image resolution | 0.17 μm/pixel |
| Image size | 1024 × 1280 pixels |
| Dynamic range | 12 bits |
| *Background subtraction* block size | 64 pixels |
| *Background subtraction* polynomial degree | 3 |
| *Alignment* maximum steps | 20 |
| *Alignment* threshold | 1.001 |
| *Alignment* step size | 1 pixel |
| *Segmentation* minimum level | 220 |
| *Segmentation* maximum level | Auto |
| *Segmentation* step size | 0.99 |
| *Segmentation* minimum size | 5 pixels |
| *Segmentation* maximum size | 9 pixels |
| *Segmentation* maximum segments per step | 150 |
| *Segmentation* maximum total segments | 0 (no limit) |
| *Analysis* CV weight | (−) 25 |
| *Analysis* slope weight | 5 |
| *Analysis* destain weight | 1 |
| *Analysis* destain point 1 | 22 (time = 42 s) |
| *Analysis* destain point 2 | 30 (time = 82 s) |
| *Analysis* minimum quality | 0.1 |

Note: The processing step of each parameter is shown in italics where appropriate.

### 3.2.4. ROI editing

Once the experiments have been automatically loaded and processed, spurious ROI (e.g., nonspecific debris) can be manually removed by the user. The ROI editing tool is shown in Supplementary Figure 2. This tool allows the user to eliminate undesired ROI or portions thereof. Automatically determined ROI are shown in Fig. 2C and D by the red and white pixels. Pixels shown in white were those that are interactively removed using the ROI editing tool. In practice, only ROI that do not fall

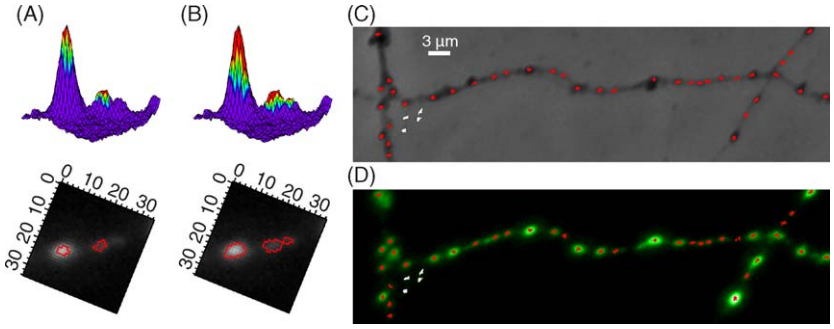


Fig. 2. Examples of segmentation: (A and B) effect of size parameters. Upper images, *Z*-axis indicates image intensity in a small XY area. Non-purple pixels were determined to be appropriate local maxima and classified as ROI. Lower images, conventional plan view of the same area with ROI outlined in red. The minimum acceptable number of contiguous pixels for an ROI was set to 5. In (A), the maximum number of contiguous pixels was set to 9 and the large peak on the left was only sampled in the center. In (B), the maximum number was 25 pixels and two small adjacent peaks on the right were considered to be a single segment. In this image the pixels represent areas 0.17 μm square. (C and D) More examples and the result of user editing. Retained (red) and erased (white) ROI are displayed over a phase contrast (C) or fluorescence (D) image. This experiment is the same as that in Figs. 3 and 4.

on neuritic processes in the transmitted light image (Fig. 2C) are removed. It is possible to exclude additional ROI on unhealthy cells or portions of cells with more aggressive manual ROI editing. In order for analysis and comparisons of experimental treatments to be objective and thereby more reproducible, however, we defer to unbiased automated ROI selection. An overlay of the ROI on the average fluorescence during the baseline period (Fig. 2D) shows many of the ROI did not fall on readily discernible fluorescent puncta, despite the somewhat saturated, high gain presentation of the fluorescence. Adjusting for still higher gain revealed that these ROI also accurately represented puncta not previously visible (cf. Fig. 4A); the high gain also obscured the size and shape of the brighter puncta due to saturation.

### 3.3. Criterion-based quality scoring and selection of FM 1–43 ROI

Once the user has edited the ROI, the program calculates the fluorescence for each of the remaining ROI for each image in the experiment. In the case of FM dye experiments, debris is usually highly stained and may be misidentified as an ROI. Off-neurite debris, as in Fig. 2C and D, may be avoided by editing, but some debris will be coincident with neuritic processes. In addition, fluorescence signals with unfavorable signal-to-noise ratio and release sites displaying a large amount of spontaneous fluorescence decay may be inappropriate for analysis. To allow the benefits of automatic segmentation without inclusion of undesirable ROI, the program has an optional additional feature to score the fluorescence change of each ROI according to three measurements: the coefficient of variation (CV) of the baseline, the slope of the baseline, and the final extent of destaining. A weighted sum of these three scores (referred to as the "quality" parameter) is calculated according to the following:

$$\begin{aligned}\text{quality} = {} & (\text{weighted, corrected slope}) \\ & +(\text{weighted fractional destaining}) \\ & -(\text{weighted baseline CV})\end{aligned}$$

The weighting of the CV is positive but shown as negative in Fig. 3 to reflect its negative relationship to quality. Slopes greater than zero are considered to be zero for scoring purposes because the slope is never positive except due to noise. For actual implementation of these scoring measures, see the program itself in the supplementary information. If the quality value does not exceed a user-specified threshold, the ROI is excluded from further analysis. This approach has been developed for styryl dye-stained preparations. It is amenable, however, to the use of synapto-pHluorin as a synaptic vesicle recycling probe and to the analysis of similar experiments requiring data selection on the basis of functionality scoring.

The retained ROI shown as red pixels in Fig. 2D were analyzed for fluorescence intensity across all the images, and the optional scoring for quality was performed. Fig. 3A shows the destaining in response to field stimulation for eight sample ROI. An ROI corresponding to a healthy release site is usually expected to have little fluorescence change during the baseline period, followed by a stimulation dependent destaining. Negatively sloping (e.g. Fig. 3A(f and g)) or noisy baselines (e.g. Fig. 3A(d, e and h)) may have a biological basis, such as a very high rate of spontaneous release, or could be due to placement of an ROI on a piece of moving debris, or may simply reflect a low fluorescence signal. In any case, the responses of such structures with especially noisy or negatively sloping baselines should be excluded in most types of experiments. Thus, values for the slope and coefficient of variation of the baseline fluorescence were used as an objective basis for data exclusion. The values of these measures for all ROI in the experiment are shown in Fig. 3B(a and b), respectively. Occasionally, ROI showed little stimulation-specific destaining, usually attributable to an already decreasing baseline (e.g. Fig. 3A(f and g)). The distribution of destaining scores is shown in Fig. 3B(c). All three score distributions show that dimmer ROI were less likely to have positive characteristics, which is expected as the noise inherent in measuring weak signals would tend to decrease the quality of the measurements. However, the correlation between intensity and slope or destaining was fairly weak above a moderate level of intensity (lines in Fig. 3B(b and c)). As expected, lower fluorescence intensity contributed to a higher baseline CV (line in Fig. 3B(a)) due to a lower signal-to-noise ratio.

After scoring the three quality parameters, a single quality score was calculated as described above for each punctum. Grouping the ROI into one of five quality score ranges, as shown in Fig. 4A, revealed that the segmentation algorithm discerned many ROI that would probably not be chosen subjectively by a manual selection method. Color coded ROI from the five quality score ranges are overlaid on a phase contrast image and a fluorescent image that is displayed to emphasize lower intensities (resulting in many saturated pixels). Note that while some of the lower intensity ROI have low quality scores, many were detected with high quality scores (a few examples are indicated by white arrows in Fig. 4A), and would likely be missed by conventional approaches, demonstrating the potential value of this approach. To qualitatively assess the effects of the quality scoring, we plotted the quality for each ROI as a function of its initial fluorescence intensity (Fig. 4B). As with the individual scores, very dim ROI were usually excluded, but most of those over a certain level were retained. Overall 61% exceeded the threshold. Average fluorescence is shown for all the ROI in each of the five ranges in Fig. 4C. It is apparent that the quality scoring successfully chooses ROI that show stimulation-dependent destaining. This is even more clear after normalization of the traces (Fig. 4D). Fitting an exponential curve to the baseline of first, third, and fifth groups and extrapolation of these curves to the ends of the experiment reveals that the lower quality ROI have both less stimulation-dependent and more stimulation-independent destaining. To further illustrate the effect of changing the minimum quality parameter and the added value of unbiased quality selection, we compared the averaged, normalized fluorescence of all puncta with that of those over the quality threshold from another experiment (Supplementary Fig. 3).

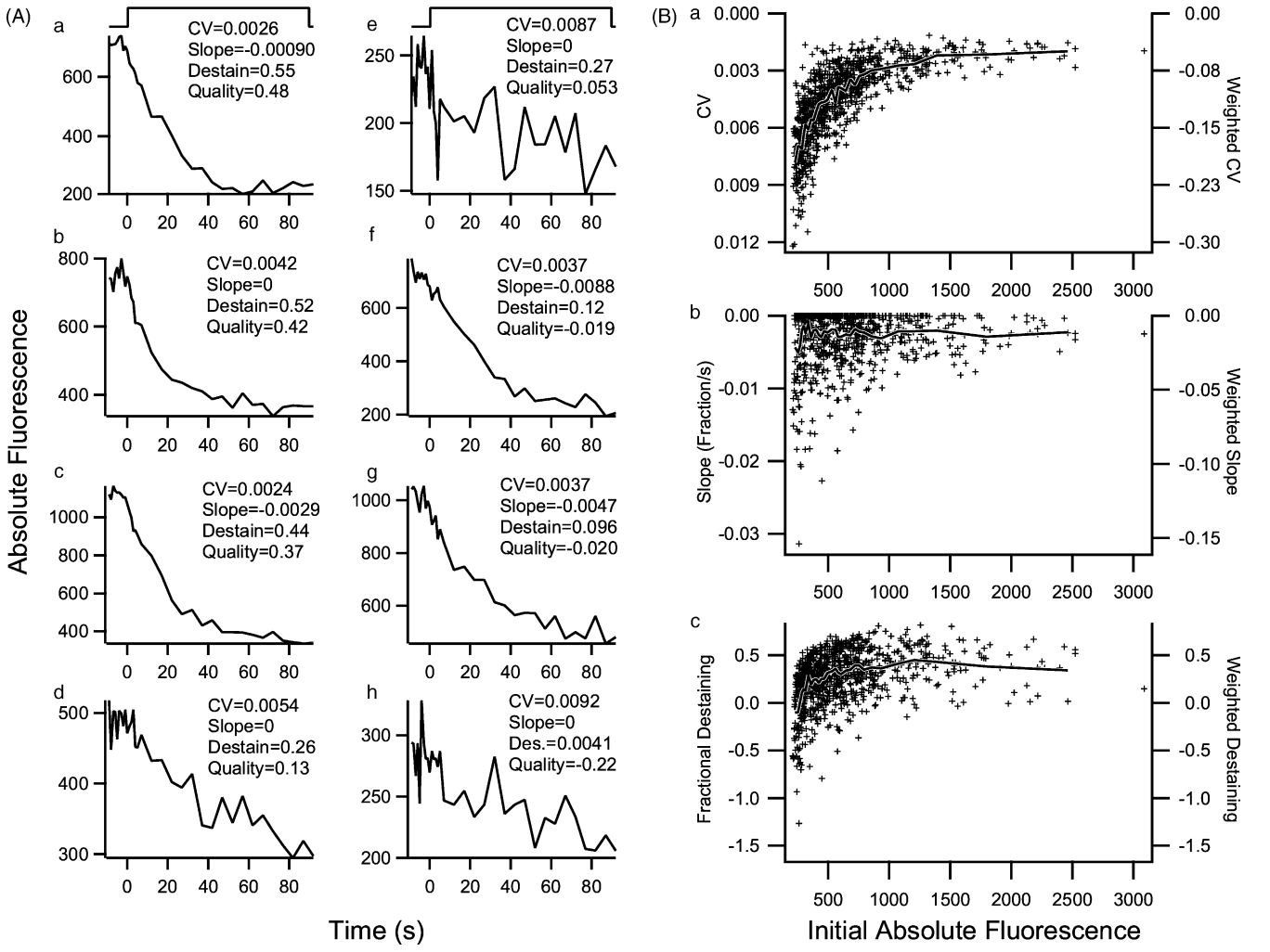


Fig. 3. Scoring for quality: (A) Eight examples of fluorescence over time for individual ROI. FM 1–43-stained cultured neurons were stimulated 900 times at 10 Hz starting at time = 0. For each the raw values of the scores used to determine quality are shown, along with the resulting quality given typical weightings (see text and Table 1). The examples in the left column (a–d) would be retained by our typical quality threshold, while those in the right column (e–h) would be rejected. The period of 10 Hz stimulation is shown above (a and e); (B) distribution of all ROI for each score as a function of the initial fluorescence (crosses). Lines indicate averages of 30 contiguous points. Raw scores are given on the left axis and typical weighted scores are given on the right axis. Note that unweighted CV (a) is plotted with larger values lower on the *Y*-axis, so that all graphs show "better" scores as upward plotting.

## 4. Summary and conclusion

The analysis of experiments using FM 1–43 or synaptopHluorin to study the function of individual synaptic release sites is usually performed with one of the numerous commercial software packages which are designed to be flexible for many types of image processing and allow the analysis of such data. Unfortunately, most involve large amounts of repetitious user intervention which is time consuming. More importantly, manual data selection and analysis introduces potential sources of bias, which may affect the validity of conclusions drawn by such strategies. Also, few commercially available image analysis packages are adequate for high level statistical analysis or yield publication-quality output, requiring further analysis and illustration in alternate software packages. We have developed a customized program allowing analysis of experiments probing synaptic function using time-lapse fluorescence microscopy with minimal user intervention running within the Igor Pro scientific software framework. Igor Pro is an inexpensive, powerful, widely used program for both Macintosh and Windows operating systems. It offers large sets of functions for image processing, mathematical data analysis, and the generation of publication-ready graphs and figures. Moreover, an extensive library of user-developed shareware exists for a variety of experimental applications.

Our open source routines allow automated background subtraction and alignment of image stacks from time-lapse fluorescence microscopy experiments probing synaptic function. They can further be used to identify and select for analysis large numbers of release sites using an automated segmentation routine. While other segmentation algorithms have been developed for the automated detection of subcellular structures (e.g. Zakharenko et al., 2002; Ponomarev and Davis, 2003; Wahlby et al., 2004 and references therein), our implementation is computationally efficient, yet very effective in detecting the small, often clustered objects with large pixel intensity variances of

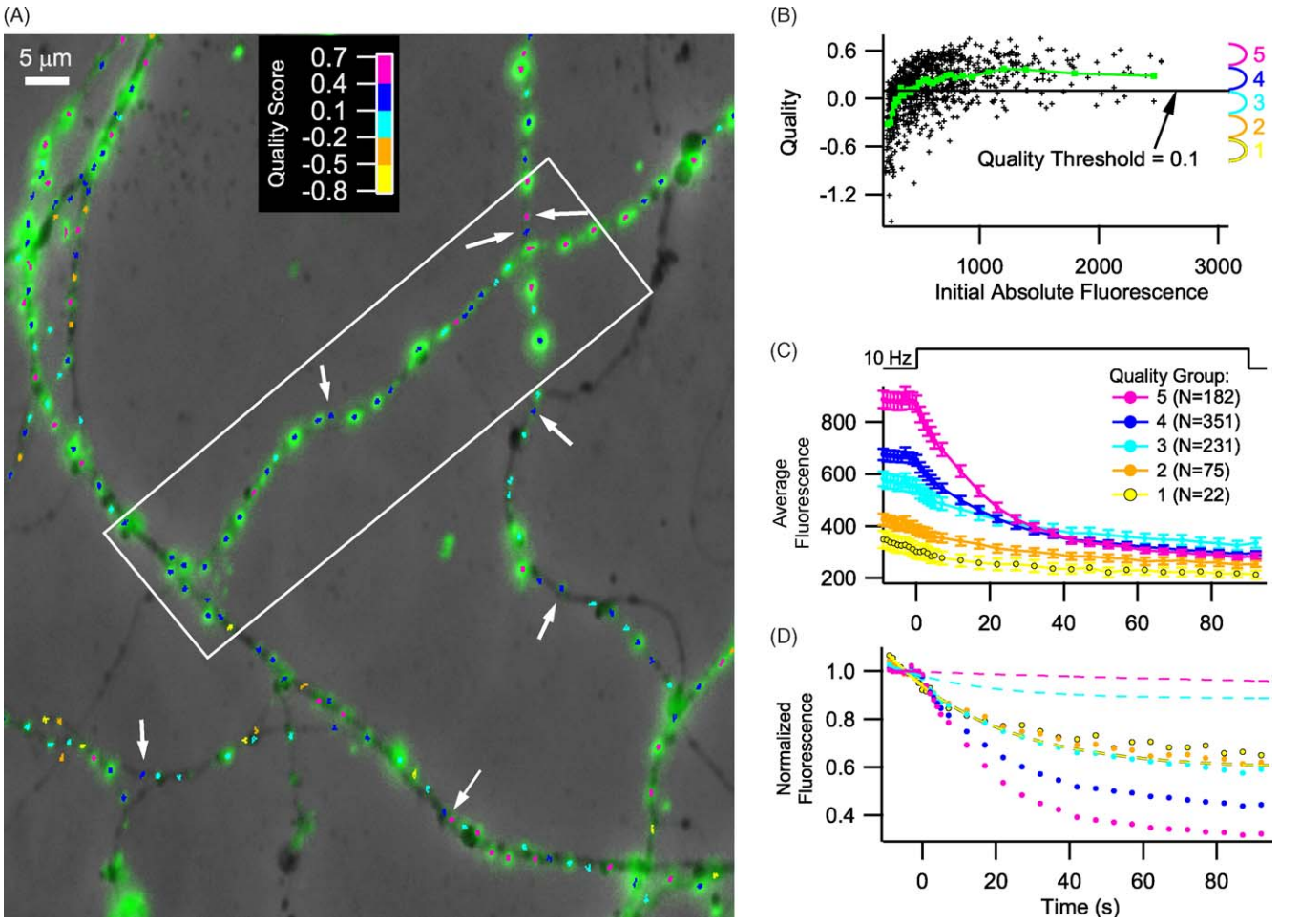


Fig. 4. Characterization of selection by quality: (A) expanded view of field from Fig. 2 with fluorescence image (green) overlaid on phase contrast image (gray). Note that the fluorescence image is displayed with high gain to reveal dim areas, resulting in many saturated areas and seemingly larger puncta. Compare to Fig. 2D. ROI are color coded into five groups according to quality score. This color code also applies to (B–D). Those in the top two groups (fuchsia and dark blue) exceeded our typical threshold. White arrows indicate examples of very low intensity release sites with high quality scores that might be missed by conventional approaches. White box outlines region depicted in Fig. 2C and D. (B) Distribution of quality for all ROI as a function of the initial fluorescence. The five quality group ranges are indicated as well as the threshold at a quality of 0.1. In this example, 61% of ROI exceeded the quality threshold. Note that other than at rather low intensity there is little relationship between intensity and quality (green trace, where each point is the average of 30 of the individual points). (C) Average fluorescence for all the ROI in each quality group. Upper trace indicates time of 10 Hz stimulation in (C and D). (D) Data from (C) normalized to baseline fluorescence (individual points). Also shown are the fit (solid lines) and extrapolated (dashed lines) baselines for groups 1, 3, and 5. Note, for example, that group 1 does not destain in response to stimulation more than predicted by the baseline.

interest in studies of synaptic vesicle cycling. Our implementation should also be very useful for other experiments exhibiting punctate fluorescence such as studies of intracellular trafficking or labeling with quantum dots.

In the development of this program, many parameters were considered and exhaustively tested. The parameters in the program fall into one of two main categories: (1) parameters that if varied or set inappropriately do not affect the robustness and accuracy of the final outcome, but do affect the user convenience or speed of processing or (2) parameters that can significantly influence the overall result of analysis. Most of the parameters are in the first category. If set grossly inappropriately, they result in slowing or complete failure of a processing step. For example, setting the alignment parameters to large numbers results in needlessly slowed processing, with no change in the overall outcome of the experiment. However, if they are set to small numbers in an experiment with a large movement of the specimen, the alignment will fail. In this case, the program alerts the user to the failure, allowing entry of new parameters for the alignment. Appropriate settings for these parameters can be determined by the user with a little experience without significantly affecting the outcome of the processing. In the second category are a few parameters that do not result in failure and do affect the outcome of the processing. However, the program is written to facilitate learning how to set these optimally (the rationale for setting optimal values is detailed in the supplemental manual).

We find that the automatic selection of release sites not only reduces the chance of human error or bias, but also greatly increases the number of release sites (typically 800-1200 ROI even in our very low density cultures) that can be analyzed from a given experiment, increasing the signal-to-noise ratio

of the data. An additional feature of our software is the ability to automatically score the fluorescence changes for each punctum according to criteria such as noise and slope of the baseline, and the amount of stimulus-induced destaining. This function allows a quick assessment of the quality of the data, and enables the experimenter to objectively and reproducibly exclude inappropriate data from further analysis based on strict and accurately applied parameters. The automated and unbiased selection and analysis operations undoubtedly increase dramatically the reproducibility and validity of experiments using fluorescent probes to study synaptic function. Indeed, our recently published observations of the novel characteristics and potential significance of dimmer release sites (Krueger et al., 2003) fully capitalized on the advantages of this automated approach, allowing us to detect and analyze fluorescently labeled synaptic structures which would typically have been overlooked using traditional analysis approaches. Beyond studying the localization and functional kinetics of FM 1–43 labeled presynaptic release sites, however, our open source software can be adapted to the analysis of fluorescent images in a wide variety of experimental paradigms.

## Acknowledgements

This work was supported by NIH (MH59800 and MH064040) grants to RMF, and an NIH training grant to JBB (T32 NS 007224-20). We thank Gawain M. Gilkey and Stephen M. Smith for the raw image in Supplementary Figure 1, Annette Kolar for her valuable technical support, and Stephen M. Smith and Larry Cohen for their valuable comments on the manuscript.

## Appendix A. Supplementary data

Supplementary data associated with this article can be found, in the online version, at 10.1016/j.jneumeth.2005.08.008.

## References

Betz WJ, Bewick GS. Optical analysis of synaptic vesicle recycling at the frog neuromuscular junction. Science 1992;255:200–3.

Krueger SR, Kolar A, Fitzsimonds RM. The presynaptic release apparatus is functional in the absence of dendritic contact and highly mobile within isolated axons. Neuron 2003;40:945–57.

Miesenböck G, De Angelis DA, Rothman JE. Visualizing secretion and synaptic transmission with pH-sensitive green fluorescent proteins. Nature 1998;394:192–5.

Miesenböck G. Imaging exocytosis with pH-sensitive green fluorescent proteins. In: Yuste R, Lanni F, Konnerth A, editors. Imaging neurons. Cold Spring Harbor, NY: Cold Spring Harbor Laboratory Press; 2000. p. 59.1–12.

Miesenböck G. Genetic methods for illuminating the function of neural circuits. Curr Opin Neurobiol 2004;14:395–402.

Pal NR, Pal SK. A review on image segmentation techniques. Pattern Recognition 1993;26:1277–94.

Ponomarev AL, Davis RL. An adjustable-threshold algorithm for the identification of objects in three-dimensional images. Bioinformatics 2003;19:1431–5.

Sahoo PK, Soltani S, Wong AKC, Chen YC. A survey of thresholding techniques. Comput Vis Graph Image Process 1988;41:233–60.

Sternberg SR. Biomedical image processing. IEEE Comput Mag 1983;16:22–34.

Wahlby C, Sintorn IM, Erlandsson F, Borgefors G, Bengtsson E. Combining intensity, edge and shape information for 2D and 3D segmentation of cell nuclei in tissue sections. J Microsc 2004;215:67–76.

Zakharenko SS, Zablow L, Siegelbaum SA. Altered presynaptic vesicle release and cycling during mGluR-dependent LTD. Neuron 2002;35:1099–110.